Int J Thermophys (2009) 30:796–809
DOI 10.1007/s10765-009-0583-5

An Accelerated Two-Dimensional Unsteady Heat Conduction Calculation Procedure for Thermal-Conductivity Measurement by the Transient Short-Hot-Wire Method

P. L. Woodfield · J. Fukai · M. Fujii · Y. Takata

Received: 21 September 2008 / Accepted: 12 April 2009 / Published online: 5 May 2009

Abstract A fast and accurate procedure is proposed for solution of the two-dimensional unsteady heat conduction equation used in the transient short-hot-wire method for measuring thermal conductivity. Finite Fourier transforms are applied analytically in the wire-axis direction to produce a set of one-dimensional ordinary differential equations. After discretization by the finite-volume method in the radial direction, each one-dimensional algebraic equation is solved directly using the tri-diagonal matrix algorithm prior to application of the inverse Fourier transform. The numerical procedure is shown to be very accurate through comparison with an analytical solution, and it is found to be an order of magnitude faster than the usual numerical solution.

P. L. Woodfield (✉) · M. Fujii
Research Center for Hydrogen Industrial Use and Storage, National Institute of Advanced Industrial Science and Technology, 744 Motooka, Nishi-ku, Fukuoka 819-0395, Japan
e-mail: p.woodfield@aist.go.jp

M. Fujii
e-mail: fujii-motoo@aist.go.jp

J. Fukai
Department of Chemical Engineering, Kyushu University, 744 Motooka, Nishi-ku, Fukuoka 819-0395, Japan
e-mail: jfukai@chem-eng.kyushu-u.ac.jp

Y. Takata
Department of Mechanical Engineering, Kyushu University, 744 Motooka, Nishi-ku, Fukuoka 819-0395, Japan
e-mail: takata@mech.kyushu-u.ac.jp

Keywords Thermal conductivity · Transient short hot wire · Two-dimensional numerical solution

1 Introduction

Transient hot-wire methods for measuring thermal conductivity are based on the principle that the transient temperature change of a fine wire, suddenly heated by a constant current, depends on the thermal properties of the surrounding fluid. The wire itself serves as both the heater and a resistance thermometer, and measurements are taken within a short time to avoid the effects of natural convection. The conventional transient hot-wire method is widely considered as the state-of-the-art technique for measurement of thermal conductivities of fluids. However, it requires a relatively large sample and two wires of different lengths to correct for end effects [1,2]. An alternative to the conventional method, known as the transient short-hot-wire method [3], uses one short wire and a numerical technique to solve the two-dimensional unsteady heat conduction equation. This method has the advantage that the apparatus is simpler than the conventional method, but has a disadvantage that additional calculation time and effort is required to ensure that numerical errors do not reduce the accuracy of the determined thermal conductivity and thermal diffusivity.

Recently, our group developed a procedure for application of the transient short-hot-wire method to data where the temperature rise of the wire does not form a straight line when plotted against the logarithm of time [4]. In order to determine the thermal conductivity via an iterative non-linear least-squares fitting procedure, the unsteady two-dimensional heat conduction equation must be solved 6–18 times. The numerical solution of the two-dimensional heat conduction equation is the time-consuming part of the procedure. Iteration is also required in solving the discretized equations themselves, and thus a convergence criterion must be employed. Since this is a possible source of discrepancy in the evaluation of the thermal properties, it is desirable to have a fast method of solving the two-dimensional heat conduction equation where iteration is not required.

In the method we propose in this article, a finite Fourier transform changes the two-dimensional problem into a set of one-dimensional problems. After discretization, the set of one-dimensional equations can be solved by direct inversion each time step using the tri-diagonal matrix algorithm (TDMA). Thus, no iteration is needed for an accurate solution of the two-dimensional unsteady heat conduction equation.

The proposed solution method has some features in common with the analytical solutions for heated cylindrical wires as described in Refs. [5] and [6]. The analytical solutions also employ finite Fourier transforms in the axial direction. However, these solutions become complicated through the analytical treatment of the radial and time derivatives. Moreover, they cannot be extended easily to coated wires. The novelty of this procedure is that it keeps the flexibility of a numerical solution in the radial direction while still taking advantage of the increased calculation speed through an analytical treatment in the axial direction.

2 Mathematical Formulation

2.1 Physical Model

The object of this method is to solve Eq. 1a subject to the initial and boundary conditions given by Eqs. 1b and c, respectively:

$$\rho c \frac{\partial T}{\partial t} = \frac{1}{r}\frac{\partial}{\partial r}\left(r\lambda\frac{\partial T}{\partial r}\right) + \lambda\frac{\partial^2 T}{\partial z^2} + Q \tag{1a}$$

$$T|_{t=0} = T|_{r=R} = T|_{z=0} = 0 \tag{1b}$$

$$\frac{\partial T}{\partial z}|_{z=L/2} = 0 \tag{1c}$$

where T is the temperature rise of the sample ($r > r_0$) or the hot wire ($r < r_0$), ρc is the volumetric heat capacity, t is the time, z is the axial direction, r is the radial direction, R is the radius of the cell, L is the length of the wire, and λ is the thermal conductivity. The power from Joule heating, Q, is defined in Eq. 2 where q is the heat supplied per unit heater length per unit time;

$$\begin{aligned} Q &= q/\pi r_0^2 \quad (r \le r_0 \text{ and } t \ge 0) \\ &= 0 \quad (r > r_0 \text{ or } t < 0) \end{aligned} \tag{2}$$

The properties of the domain vary according to Eqs. 3 and 4 where r_0 is the radius of the wire and the subscript, w, stands for the wire while the subscript, s, is for the sample;

$$\lambda|_{r\le r_0} = \lambda_w, \lambda|_{r>r_0} = \lambda_s \tag{3}$$

$$\rho c|_{r\le r_0} = \rho_w c_w, \rho c|_{r>r_0} = \rho_s c_s \tag{4}$$

A schematic diagram of Eqs. 1–4 is given in Fig. 1.

2.2 Fourier Transform in Axial Direction

Equation 1 is written such that it is valid for changes in properties in the radial direction but not in the axial direction. This assumption allows us to apply a finite Fourier

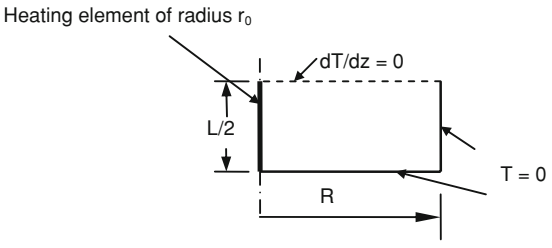

Fig. 1 Physical model

transform in the z direction. Thus we can make use of the following finite Fourier transform:

$$\bar{f}(z) = \int_0^{L/2} \sin(m_n z)\, f(z)\, \mathrm{d}z \tag{5}$$

$$m_n = \frac{2n-1}{L}\pi, \quad n = 1, 2, 3\ldots \tag{6}$$

The inverse Fourier transform is given by

$$f(z) = \frac{4}{L}\sum_{n=1}^{\infty} \sin(m_n z)\, \bar{f}(z) \tag{7}$$

Applying Eq. 5 to Eqs. 1a, b, and c and assuming properties do not vary in the z direction, we obtain

$$\rho c \frac{\partial \bar{T}_n}{\partial t} = \frac{1}{r}\frac{\partial}{\partial r}\left(r\lambda \frac{\partial \bar{T}_n}{\partial r}\right) - \lambda m_n^2 \bar{T}_n + \frac{Q}{m_n} \tag{8a}$$

$$\bar{T}_n|_{t=0} = 0 \tag{8b}$$

$$\bar{T}_n|_{r=R} = 0 \tag{8c}$$

Note that the two-dimensional unsteady problem given by Eq. 1 is now N one-dimensional unsteady problems given by Eq. 8 where $n = 1, N$.

2.3 Numerical Discretization in Time and Radial Direction

Equation 8a is discretized using the finite-volume method [7] with central differencing for the first term on the right and a fully implicit scheme for the unsteady term on the left. The term $-\lambda m_n^2 \bar{T}_n$ in Eq. 8a is treated implicitly while the term Q/m_n is treated as an explicit source term. This results in a tri-diagonal matrix. Thus, Eq. 8 can be solved very quickly without iteration for different values of 'n' using the well-known TDMA. Contrary to Ref. [7], in this study, we have used node-centered control volumes. The formulation is a little more complicated than the cell-centered approach, but it avoids some ambiguity in the treatment of thermal conductivity at the boundary between the wire and the fluid sample. Details of our discretization method are given in the Appendix.

2.4 Inverse Fourier Transform

Having obtained a sufficiently large number of values of $\bar{T}_n$, the temperature (see Eq. 7) at any position is given by

$$T(r,z,t) = \frac{4}{L}\sum_{n=1}^{\infty} \sin(m_n z)\,\bar{T}_n(r,t) \tag{9}$$

The average temperature in the wire at time, t, is given by Eq. 10 where we have integrated Eq. 9 from $z = 0$ to $L/2$ and from $r = 0$ to r_0 and then divided by the volume of the wire. Note that the Fourier series has been truncated to N terms;

$$T_{\mathrm{w}}(t) = \frac{8}{L^2}\sum_{n=1}^{N}\frac{1}{m_n}\frac{2}{r_0^2}\int_0^{r_0}\bar{T}_n(r,t)\,r\,\mathrm{d}r \tag{10}$$

3 Extensions to the Procedure

3.1 Modification for a Constant-Current Supply

In the previous section, the Joule heating per unit length of the wire, q, is treated as a constant value. This is the usual assumption for the transient hot-wire method [1–4], but it is not necessary to limit the present procedure to this assumption. Actually, in the practical apparatus, a constant-current source is typically used. The present procedure can easily be reformulated for a constant current. In order to do this, q in Eq. 2 is replaced by

$$q = \frac{I^2 R_{0\mathrm{C}}(1+\beta T_0)}{L} + \frac{I^2 R_{0\mathrm{C}}\beta}{L}T \tag{11}$$

where I is the electrical current, $R_{0\mathrm{C}}$ is the resistance of the wire at 0 °C, β is the resistance coefficient for the wire, and T_0 is the bath temperature at the start of the experiment. Substituting Eq. 11 into Eq. 1a and applying the finite Fourier transforms gives

$$\rho c\frac{\partial \bar{T}_n}{\partial t} = \frac{1}{r}\frac{\partial}{\partial r}\left(r\lambda\frac{\partial \bar{T}_n}{\partial r}\right) - \lambda m_n^2 \bar{T}_n + \frac{I^2 R_{0\mathrm{C}}(1+\beta T_0)}{\pi r_0^2 L m_n} + \frac{I^2 R_{0\mathrm{C}}\beta}{\pi r_0^2 L}\bar{T}_n \tag{12}$$

As per the recommendation of Ref. [7] concerning positive and negative source terms in the finite-volume method, the last two terms on the right-hand side of Eq. 12 are discretized explicitly by taking the value of $\bar{T}_{\mathrm{n}}$ from the previous time step. Thus, for the case of a constant current, Eq. 12 should be solved in place of Eq. 8a.

3.2 Application to Wires with Protective Coatings

This procedure can be extended easily for application to a wire covered by a protective coating such as that which was used in Ref. [8]. To apply the finite Fourier transforms to Eq. 1, it is only necessary that the thermal conductivity and heat capacity do not vary in the axial direction. There is no restriction on property variation in the

radial direction. Therefore, the conditions in Eqs. 3 and 4 can easily be changed to the following:

$$\lambda|_{r\le r_0} = \lambda_w \qquad \lambda|_{r_0<r\le r_c} = \lambda_c \qquad \lambda|_{r>r_c} = \lambda_s \tag{13}$$

$$\rho c|_{r\le r_0} = \rho_w c_w \qquad \rho c|_{r_0<r\le r_c} = \rho_c c_c \qquad \rho c|_{r>r_c} = \rho_s c_s \tag{14}$$

where the subscripts, w, is for the heating element, c is for the coating, and s is for the sample.

4 Demonstration of the Procedure

4.1 Calculation Speed and Accuracy for Application to Gas with High Thermal Diffusivity

It is worthwhile to consider fluids with both high and low thermal diffusivities since the wire temperature-rise characteristics are quite different for the extremes of thermal diffusivity [4]. Table 1 gives a comparison of this procedure with the two-dimensional finite-volume method where both are applied for simulation of a short wire surrounded by hydrogen gas at atmospheric pressure. For this example, the properties of the sample were taken to be $\lambda = 0.183\,\mathrm{W\cdot m^{-1}\cdot K^{-1}}$, $\alpha = 1.525\times10^{-4}\,\mathrm{m^2\cdot s^{-1}}$, and of the wire $\lambda_w = 71.6\,\mathrm{W\cdot m^{-1}\cdot K^{-1}}$, $\alpha_w = 2.51\times10^{-5}\,\mathrm{m^2\cdot s^{-1}}$. Low-pressure hydrogen gas was selected as an extreme case of a high thermal-diffusivity fluid. The electrical current to the wire was 15 mA, corresponding to a heating power of $0.29504\,\mathrm{W\cdot m^{-1}}$. The cell geometry is included in Fig. 2. Calculations were performed for three different values of N corresponding to the number of terms in the Fourier series in Eq. 10. The first grid space in the fluid in the radial direction is 0.27 times the radius of the wire, and subsequent grid spaces increase in size according to a geometric progression. Time steps also increase geometrically from a first step of 50 μs in the same manner as explained in Ref. [4]. Calculations were done on a Pentium D personal computer with 3-GHz clock speed. The calculation time in Table 1 includes the time taken to write the output into the hard disk.

From Table 1 it is clear that for this example, $N = 50$, in this method results in a similar accuracy to the 2D finite-volume method with $N_z = 38$. For this case, the calculation time taken in this method is less than one-tenth of that taken in the 2D

Table 1 Comparison with 2D finite-volume method for H_2 gas

	N_r	N_t	Calculation time (s)	Steady state T (K)	T (K) at $t = 0.1$ s
2D FVM ($N_z = 38$)	320	1800	152	1.64442	1.61619
Present $N = 50$	320	1800	11	1.64458	1.61632
Present $N = 100$	320	1800	15	1.64467	1.61642
Present $N = 200$	320	1800	28	1.64468	1.61643
2D Analytical [5]	–	–	–	1.64539	1.61722

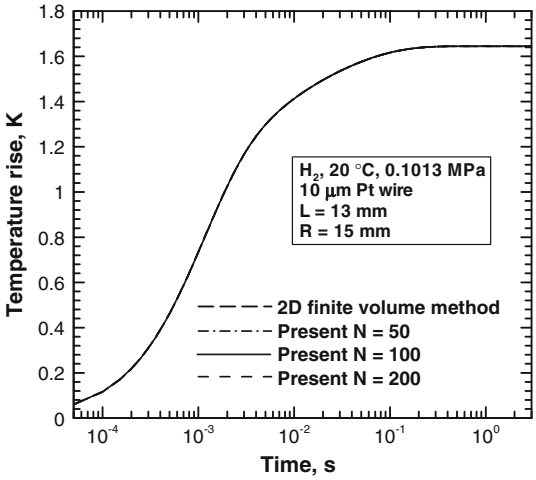

Fig. 2 Volume-averaged wire temperature rise for hydrogen gas

finite-volume method. The analytical solution [5] to the same problem (but neglecting the radial temperature gradient in the wire) is also listed in Table 1. The steady-state numerical results are all within 1 mK of the analytical solution. Moreover, the results of this method are slightly closer to the analytical solution than those of the 2D finite-volume solution. Differences between the numerical and analytical solutions can be reduced even further by increasing the number of points in the radial direction and increasing the number of time steps.

Figure 2 shows the volume-averaged temperature rise for the four numerical simulations considered in Table 1. It is difficult to distinguish between the four cases as should be expected based on the results shown in Table 1. Figure 3 shows the result of calculating the temperature distribution in the sample with Eq. 9 (the number of terms is $N = 100$) and the result from the 2D finite-volume method. The maximum difference in temperature rise between the two distributions in Fig. 3 is 5.9×10^{-3} K while the average absolute difference is 0.1×10^{-3} K. The maximum difference between the two distributions occurs at $r = 0$ and $z = 0.025$ mm, which is the first z-grid point in the wire.

Since the temperature distribution in the wire itself has a direct influence on the resistance measurement, it is also worthwhile to confirm the absence of significant oscillations from the finite-Fourier series. Figure 4 shows the temperature distribution along the axis of the wire calculated using this method and the 2D finite-volume method. The average absolute difference at grid points along the wire axis is about 0.6×10^{-3} K which is slightly larger than the difference in the volume averages shown in Table 1. Temperature oscillations along the wire greater than the order of 1 mK are absent. Thus, Figs. 2–4 verify the accuracy of this procedure when applied to a high thermal-diffusivity gas.

4.2 Performance for a Fluid with Low Thermal Diffusivity

The thermal diffusivity of liquids such as toluene and water is several orders of magnitude lower than that of hydrogen gas at atmospheric pressure. This has the effect

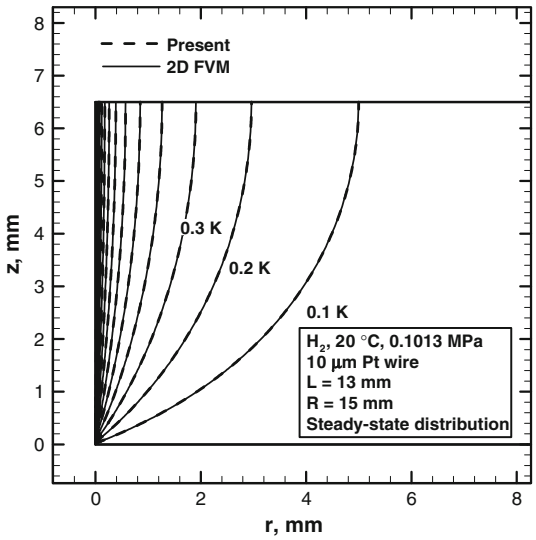

Fig. 3 Comparison of steady-state temperature distribution using Eq. 9 with 2D FVM

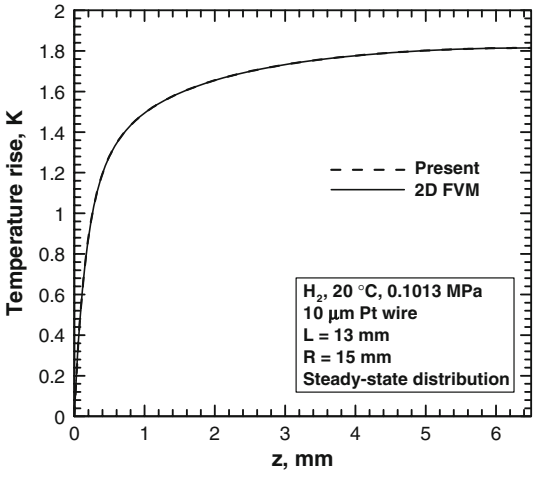

Fig. 4 Steady-state temperature distribution along the axis of the wire

that only a small region very close to the wire is heated during an experiment, and thus the boundary conditions at the cell walls become irrelevant. Table 2 shows a comparison between this method, the 2D finite-volume method, and an analytical solution for the case of liquid toluene at 20 °C. Properties of toluene were taken to be $0.1324\,\mathrm{W\cdot m^{-1}\cdot K^{-1}}$ and $9.124\times10^{-8}\,\mathrm{m^2\cdot s^{-1}}$ for thermal conductivity and thermal diffusivity, respectively. The heating power ($0.29504\,\mathrm{W\cdot m^{-1}}$) and computational grids were the same as those used for hydrogen gas above. Again, the agreement between this method and the 2D finite-volume method is within 1 mK at the sample points for all the cases considered. The results from the analytical solution are

Table 2 Comparison with 2D finite-volume method for liquid toluene

	N_r	N_t	Calculation time (s)	T (K) at $t = 1$ s	T (K) at $t = 0.1$ s
2D FVM ($N_z = 38$)	320	1800	66	1.54808	1.15909
Present $N = 50$	320	1800	11	1.54815	1.15913
Present $N = 100$	320	1800	15	1.54824	1.15923
Present $N = 200$	320	1800	28	1.54826	1.15924
2D Analytical [5]	–	–	–	1.54940	1.16042

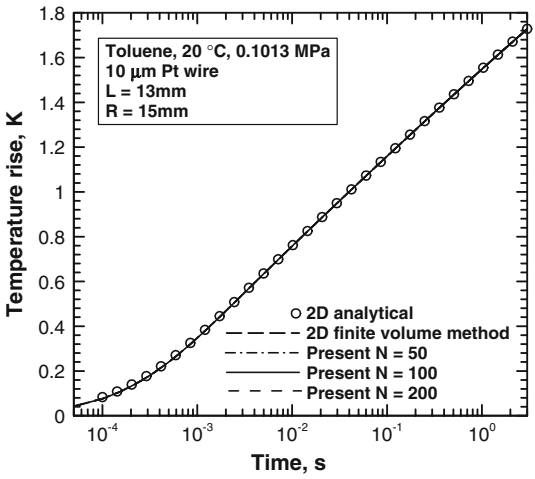

Fig. 5 Volume-averaged wire temperature rise for liquid toluene

about 1.2 mK greater than the numerical results. A comparison between Tables 1 and 2, shows that the calculation times for this method are unchanged. This should be expected since this procedure does not require iterations for convergence. The 2D finite-volume solution converges faster for toluene (66 s) than for hydrogen (152 s). Even then, this procedure still indicates a significant improvement to the calculation time.

Figure 5 shows the wire temperature rise for the cases listed in Table 2. In contrast to the case for hydrogen in Fig. 2, Fig. 5 shows a linear relationship between the temperature rise and the logarithm of time. For hydrogen gas, the wire temperature reaches a steady state due to the effects of the cell wall boundary. This effect is not seen in the case of toluene because of the much smaller thermal diffusivity. The good agreement among the various calculations over the entire transient temperature rise in Fig. 5 is consistent with the results reported in Table 2. It is worth mentioning that the analytical solution in Ref. [5] is most suitable for fluids with high thermal diffusivity and for large values of t. In the case of Fig. 5 for $t < 1$ ms, 2000 terms per eigenvalue were required for the analytical solution to converge. This is a further motivation for the use of this procedure in preference to the analytical solution in Ref. [5].

4.3 Effect of Constant-Power Assumption

Usually, in the transient hot-wire method it is assumed that throughout the duration of the experiment the power to the wire remains constant. However, in the actual experiment a constant-current source is normally used. In the case of a constant current, the resistance of the wire changes slightly as the temperature increases and thus the power increases slightly with time. In Sect. 3.1 we showed that the present numerical solution can be altered easily for the case of a constant current. If the temperature rise is less than 1 K, the change in the resistance of a platinum wire is less than 0.4 %. (Note that for high-purity platinum, $\beta \approx 0.0039\,\mathrm{K}^{-1}$). The effect on the thermal-conductivity measurement is smaller than this if the time-averaged resistance is used to specify the power. Occasionally, transient hot-wire data appear in the literature where the temperature rise is greater than 5 K. Therefore, we will consider such a case here in order to represent an upper limit used in practical measurements.

Figure 6 shows the simulated wire temperature rise in hydrogen gas for a constant current of 40 mA in a transient short-hot-wire cell with a 10 μm diameter platinum wire. For comparison, constant-power simulations are done using the time-averaged resistance (dashed line) and the initial resistance (dashed-dotted line) to estimate the power per unit length. We can see from Fig. 6 that even in the case of a temperature rise of about 8 K, the constant-current and constant-power curves are in good agreement if the average power is used. The largest difference between the average-power result and the constant-current result is about 0.077 K at $t \approx 1.5$ ms. For the steady-state condition the difference is 0.0056 K. On the other hand, if the initial resistance is used to estimate the power, the maximum difference is 0.24 K and an error of the order of 3 % in thermal conductivity could result for this case. Thus, we may conclude that the main advantage of using Eq. 12 (i.e., constant current) is to avoid ambiguity in specification of the power to the wire.

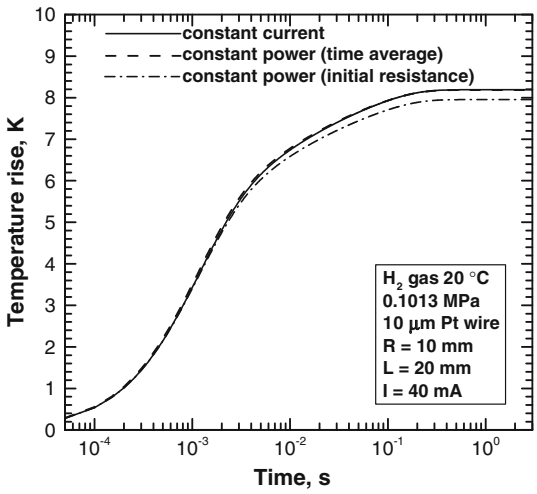

Fig. 6 Effect of constant-power assumption

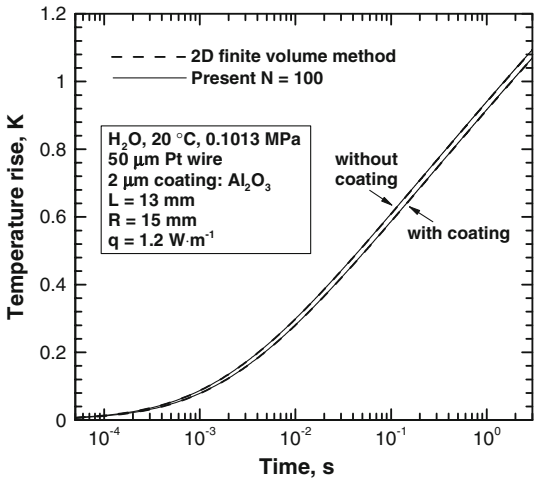

Fig. 7 Coated-wire simulation

4.4 Coated Wires

As mentioned above, the transient short-hot-wire method has been applied to measurement of electrically conducting fluids by application of a layer of Al_2O_3 on the surface of the wire [8]. In order to demonstrate the validity of the present procedure for such application, Fig. 7 shows simulation results of the volume-averaged wire temperature rise for a platinum wire with and without an Al_2O_3 coating. For this example, the test fluid was water at 20 °C, 0.1013 MPa, with IAPWS recommended properties as formulated in NIST's software REFPROP [9]. The properties of the coating have a large degree of uncertainty as a result of the sputtering procedure. For this simulation, the thermal conductivity and thermal diffusivity of the Al_2O_3 coating were assumed to be $36\,\mathrm{W \cdot m^{-1} \cdot K^{-1}}$ and $11.9 \times 10^{-6}\,\mathrm{m^2 \cdot s^{-1}}$, respectively. The present method was implemented as described above in Sect. 3.2. For this case as shown in Fig. 7, the coating has the effect of reducing the temperature rise. Again, the simulations using the 2D finite-volume discretization differ by less than 1×10^{-3} K from the corresponding results using the present procedure.

5 Limitations of the Present Model

The numerical technique described in this article is limited to thermal-conductivity cells where the geometry can be approximated such that the boundary conditions at $z = 0$ and $z = L/2$ do not vary with r. Moreover, properties cannot vary in the z-direction. This may seem a little restrictive but the models usually used for the transient short-hot-wire method satisfy all of these conditions [3,8]. Moreover, the model outlined in this article has been used with considerable success for the measurement of the thermal conductivities of liquids [3,8,10]. However, it should be noted that due to difficulties in the construction of a short-hot-wire cell, the physical model in Fig. 1 is not a perfect representation of geometry used in practice for the transient short-hot-wire

method. It is also difficult to measure the length of the wire with an optical microscope due to uncertainties about the weld attachment positions on the lead terminals [3]. In order to overcome this problem and to compensate for any differences between the model and the experiment, the transient short-hot-wire method is usually treated as a secondary method. The cell constants are an effective wire length and an effective diameter that are determined via calibration measurements in a reference fluid such as liquid water or toluene where the properties are well known [3,8]. For liquids, the sample is heated only in the region very close to the wire. For high-diffusivity gases such as low-density hydrogen, however, the heated region extends all the way to the cell wall, as is evident from the steady-state condition reached in Fig. 2. Therefore, we may expect that model differences with respect to details of the cell geometry in the lower and upper parts of the cell far from the wire will be more significant for gases than for liquids. Thus, it is important to mention that calibration in a fluid with similar properties may be required if the present physical model is applied to low-density gases.

6 Conclusions

This proposed method is a useful modification to the calculation procedure for the transient short-hot-wire method. Not only is the calculation time reduced but also some numerical convergence issues are avoided through direct inversion of the algebraic equations using the TDMA. It is also applicable to coated wires and to constant-current power sources.

Acknowledgments This research has been conducted as a part of the "Fundamental Research Project on Advanced Hydrogen Science" funded by the New Energy and Industrial Technology Development Organization (NEDO).

Appendix

Numerical Discretization in the Radial Direction

Since the node-centered finite-volume treatment used in the present article is a little less common than the cell-centered approach, it is worthwhile to give a brief description of the procedure used here. The goal is to discretize the following equation:

$$\rho c \frac{\partial \bar{T}_n}{\partial t} = \frac{1}{r}\frac{\partial}{\partial r}\left(r\lambda \frac{\partial \bar{T}_n}{\partial r}\right) - \lambda m_n^2 \bar{T}_n + \frac{Q}{m_n}$$

In order to simplify the notation, let T_i be the value of the Fourier transform of the temperature at the position $r = r_i$;

$$T_i \equiv \bar{T}_n|_{r=r_i}$$

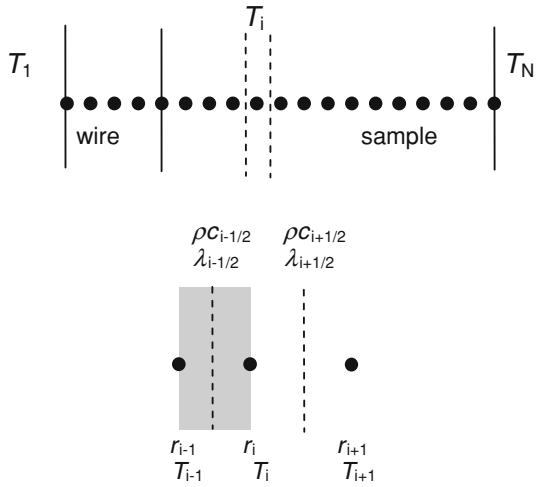

Fig. 8 One-dimensional numerical grid definitions

Figure 8 gives a schematic diagram of a single control volume. The solid circles show the positions at which the temperature (i.e., Fourier transform of the temperature) is evaluated while the dashed lines show the positions at which the properties are specified. The dotted lines also correspond to the boundaries of the control volume. Note that the dotted line is halfway between two solid circles, but the solid circles are not necessarily halfway between the two dotted lines. In order to be generic, the left part of the control volume is taken to have different properties to the right part of the control volume. This is illustrated by the shading in Fig. 8. The discretized equation for the node i becomes

$$
\begin{aligned}
&\frac{\rho_{i-1/2}c_{i-1/2}\pi\left(r_i^2-((r_i+r_{i-1})/2)^2\right)}{\Delta t}\left(T_i-T_i'\right)\\
&+\frac{\rho_{i+1/2}c_{i+1}\pi\left(((r_{i+1}+r_i)/2)^2-r_i^2\right)}{\Delta t}\left(T_i-T_i'\right)\\
&+\lambda_{i-1/2}m_n^2\pi\left(r_i^2-((r_i+r_{i-1})/2)^2\right)T_i\\
&+\lambda_{i+1/2}m_n^2\pi\left(((r_i+r_{i+1})/2)^2-r_i^2\right)T_i\\
&-\left(Q_{i-1/2}/m_n\right)\pi\left(r_i^2-((r_i+r_{i-1})/2)^2\right)\\
&-\left(Q_{i+1/2}/m_n\right)\pi\left(((r_i+r_{i+1})/2)^2-r_i^2\right)\\
&+2\pi\frac{(r_i+r_{i-1})}{2}\frac{\lambda_{i-1/2}}{r_i-r_{i-1}}\left(T_i-T_{i-1}\right)\\
&-2\pi\frac{(r_{i+1}+r_i)}{2}\frac{\lambda_{i+1/2}}{r_{i+1}-r_i}\left(T_{i+1}-T_i\right)=0
\end{aligned}
\tag{A1}
$$

Δt is the numerical time step, and T_i' is the temperature at grid point i at the end of the previous time step. It is also worth mentioning that double floating point precision was used in the computer program to implement this solution.

References

1. Y. Nagasaka, A. Nagashima, Rev. Sci. Instrum. **52**, 229 (1981)
2. J.J. Healy, J.J. de Groot, J. Kestin, Physica **82C**, 392 (1976)
3. M. Fujii, X. Zhang, N. Imaishi, S. Fujiwara, T. Sakamoto, Int. J. Thermophys. **18**, 327 (1997)
4. P.L. Woodfield, J. Fukai, M. Fujii, Y. Takata, K. Shinzato, Int. J. Thermophys. **29**, 1299 (2008)
5. P.L. Woodfield, J. Fukai, M. Fujii, Y. Takata, K. Shinzato, Int. J. Thermophys. **29**, 1278 (2008)
6. W.T. Kierkus, N. Mani, J.E.S. Venart, Can. J. Phys. **51**, 1182 (1973)
7. S.V. Patankar, *Numerical Heat Transfer and Fluid Flow* (Hemisphere, New York, 1980)
8. X. Zhang, M. Fujii, Int. J. Thermophys. **21**, 71 (2000)
9. E.W. Lemmon, M.L. Huber, M.O. McLinden, NIST Standard Reference Database 23: Reference Fluid Thermodynamic and Transport Properties-REFPROP, Version 8.0 (National Institute of Standards and Technology, Standard Reference Data Program, Gaithersburg, MD, 2007), (www.nist.gov/srd/nist23.htm)
10. X. Zhang, W. Hendro, M. Fujii, T. Tomimura, N. Imaishi, Int. J. Thermophys. **23**, 1077 (2002)